

Excited-state Quenching Phenomena in Weakly Ionised Nitrogen

A. Ernest,^A S. C. Haydon^A and M. T. Elford^B

^A Department of Physics, University of New England, Armidale, N.S.W. 2351.

^B Atomic and Molecular Physics Laboratories, Research School of Physical Sciences, Australian National University, G.P.O. Box 4, Canberra, A.C.T. 2601.

Abstract

A number of studies of the ionisation behaviour of molecular nitrogen have revealed the importance of $N_2(A^3\Sigma_u^+)$ metastable particles which are created by direct electron impact excitation or cascade processes. More recent studies using cleaner gas samples have indicated that the ionisation current may be affected by the presence of a second metastable particle. The possible identity of this second metastable particle and the sensitivity of the ionisation current to its presence have been investigated by observing the changes in the pre-breakdown ionisation current as a function of the purity of the N_2 gas samples. Both the spatial and temporal behaviour of the ionisation current were observed. Particular care was required in this study to ensure that stable electrode surface conditions were obtained and the procedures adopted are described in detail. The addition of CO and H_2 to the N_2 samples at the parts per million level confirmed the dominant quenching action of CO. Further consideration of the spatial growth of ionisation has demonstrated that an ionisation mechanism involving both $N_2(A^3\Sigma_u^+)$ and $N_2(a'^1\Sigma_u^-)$ particles provides a plausible explanation for the observations and should be further investigated.

1. Introduction

Despite considerable effort, values of the ionisation parameters in N_2 remained uncertain for many years (Folkard and Haydon 1973). A major advance in the understanding of the wide discrepancies came from the recognition of the dominating influence of metastable particles (Krisch 1968; Haydon and Williams 1972, 1973*a*), and this led in turn to more precise determinations of primary ionisation coefficients (Haydon and Williams 1976). Using 'pure' gas handling facilities, base pressures of $\sim 10^{-7}$ mbar (1 mbar \equiv 100 Pa) and modest baking procedures, it was demonstrated that the $N_2(A^3\Sigma_u^+)$ metastable particle, with an energy of ~ 6.17 eV, contributed significantly to both the spatial and temporal growth of ionisation through its diffusion to the boundary walls and its release of secondary electrons. The diffusion coefficient D was obtained using the analytical procedures of Molnar (1951*a*, 1951*b*) and was consistent with this particular metastable particle being responsible for the phenomena observed.

The ionisation behaviour of N_2 was considered to be so well understood that it was used for calibration purposes in connection with the inert gases. It is well known that in the inert gases impurity effects dominate the ionisation behaviour and consequently

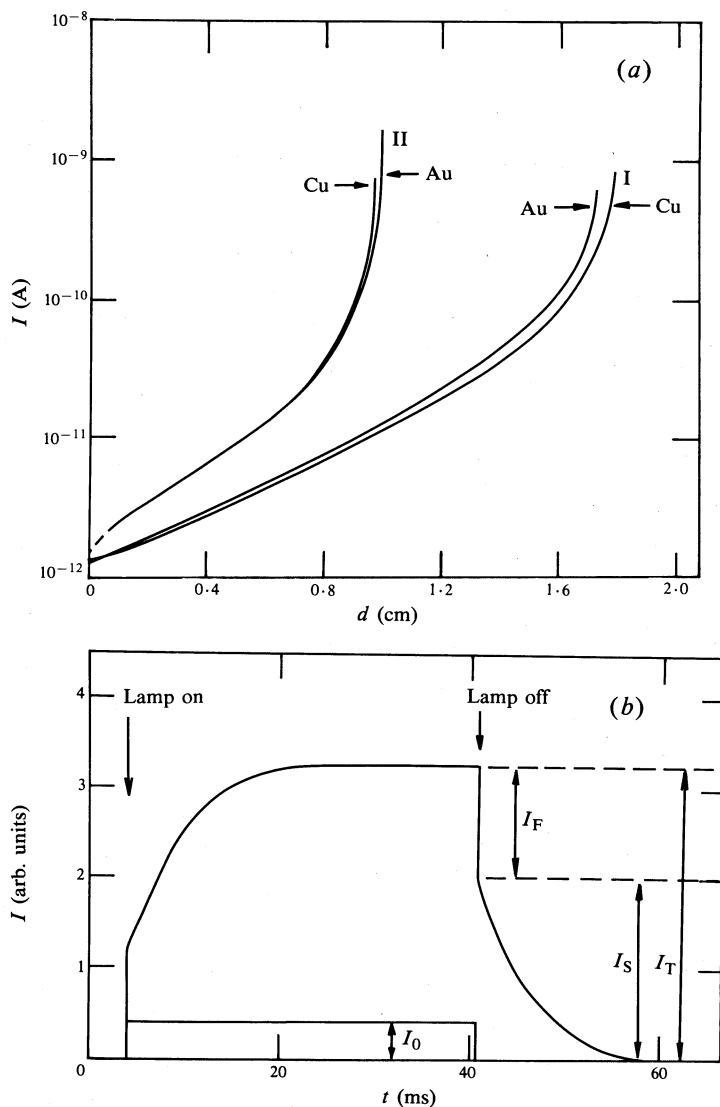


Fig. 1. (a) Curves of ionisation current I versus electrode separation d for $E/p = 100 \text{ V cm}^{-1} \text{ Torr}^{-1}$ ($E/N = 282.8 \text{ Td}$) and $p = 5 \text{ Torr}$ for the unbaked (I) and baked UHV (II) systems. (b) Schematic representation of a typical I versus t curve where I_T is the total ionisation current, I_F the fast component of the total current, I_S the slow (metastable particle) component of the total current, and I_0 the initial current from the cathode surface generated by an external Hg-vapour lamp.

more prolonged outgassing procedures were adopted for these studies. However, a consequence of the subsequent lower outgassing rate of the vacuum system was a remarkable change in measurements of the characteristic ionisation behaviour in N_2 . In particular the discharge current was found to be much larger at long times after the photo-electron source had been turned off than could be accounted for by the

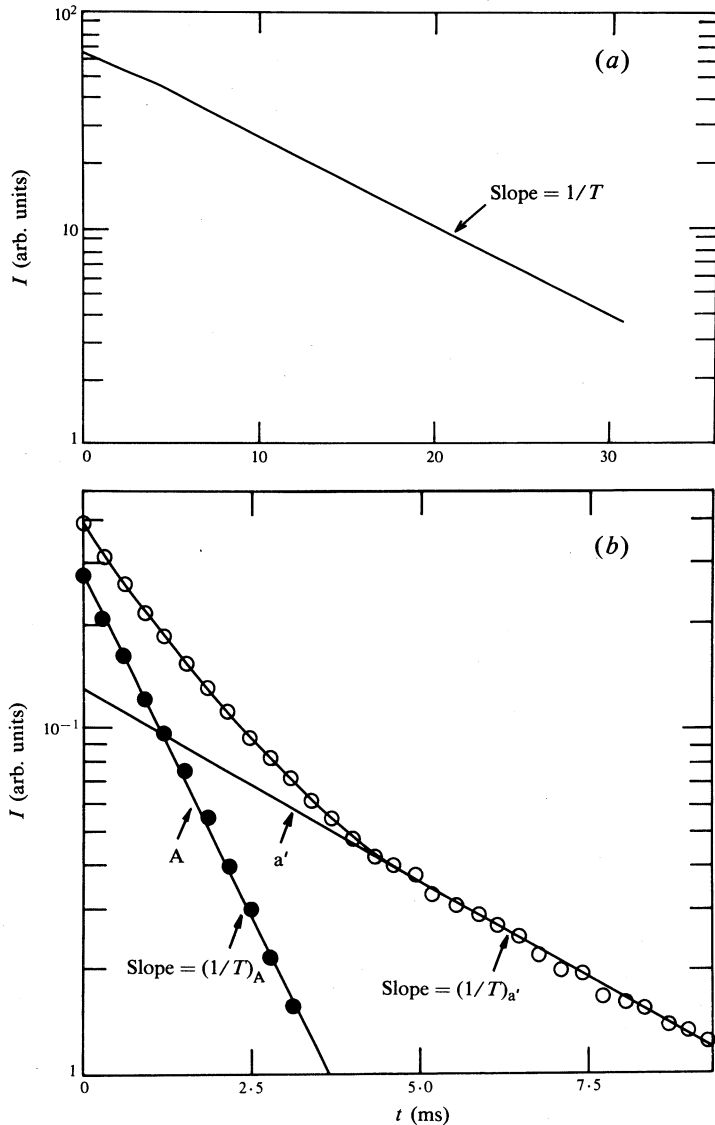


Fig. 2. (a) Plot of $\ln I$ against t yielding a current decay constant $1/T$ for $N_2(A^3\Sigma_u^+)$ metastable particles in unbaked or moderately baked systems. The conditions were $E/N = 283$ Td, $p = 5$ Torr and $d = 1.7$ cm. (b) Curve of $\ln I$ against t (open circles) for the combined contribution of two metastable particles in a UHV system after outgassing. The curve A (solid circles) is obtained by subtracting a' from the total curve. The conditions were the same as in (a) except $d = 0.52$ cm.

presence of the $N_2(A^3\Sigma_u^+)$ metastable particles alone. The Molnar (1951*a*) analysis suitably adjusted to examine temporal ionisation dominated by two metastable particles (Ernest and Haydon 1983) was used to isolate the direct contribution to the ionisation current due to the $N_2(A^3\Sigma_u^+)$ particle, the remaining ionisation

current being attributed to a second metastable particle, whose diffusion coefficient [at a pressure of 1 Torr at 273 K (1 Torr \equiv 133 Pa)] was measured as $\sim 40 \text{ cm}^2 \text{ s}^{-1}$. These preliminary experiments were unable to identify the second particle or to establish mechanisms by which the presence of small traces of impurities quenched the unidentified metastable neutral gas molecule.

Throughout the investigations the precise role of the boundary electrode surfaces has been difficult to establish. When the earliest observations were made the cathode surface was either a thin gold film or a bulk copper electrode and very different behaviour was noted in each case. Subsequently, when the original boro-silicate glass ionisation chamber was replaced by a stainless-steel UHV system, the differences in the behaviour of the two surfaces were much smaller. In nearly all of the experiments the ionisation currents were larger with the Au-film cathode, but occasionally the reverse was observed. Furthermore, and depending on both the history of the electrode surfaces and the outgassing procedures, the critical breakdown voltages varied from ~ 500 to 1200 V. The causes of such large changes have not been easy to establish and the lack of reproducibility of the surface conditions has complicated the interpretation of the observations. Whilst it is clear that the ionisation currents are very sensitive to the state of the surfaces it has not been possible to establish the corresponding sensitivity to impurity molecules in the gas volume. The need to assess the relative importance of these two effects became more important when our temporal measurements indicated the possibility that more than one metastable particle may be contributing to the ionisation growth.

The purpose of the present paper, therefore, is to clarify some of the ambiguities of interpretation that have arisen. Specifically, procedures are described in Section 3 that have led to some control over surface conditions. This, in turn, leads in Section 4 to a clearer assessment of the impurity effects responsible for the quenching mechanisms operative in pre-breakdown investigations in nitrogen. In Sections 5 and 6 we examine whether a single metastable particle mechanism could account for the observations and consider also the plausibility of two-particle processes being able to account for the observed spatial and temporal growth of ionisation in N_2 gas.

2. Spatial and Temporal Characteristics of the Ionisation Growth

Fig. 1*a* illustrates the dramatic changes brought about by the use of prolonged outgassing procedures using a stainless-steel ionisation chamber with thin gold film and bulk copper electrodes. The curves show the ionisation current I as a function of the electrode gap separation (plane-parallel geometry) for the same values of $E/p = 100 \text{ V cm}^{-1} \text{ Torr}^{-1}$ ($E/N = 282.8 \text{ Td}$; $1 \text{ Td} \equiv 10^{-17} \text{ V cm}^2$). All pressures, throughout the investigation, have been corrected to values at $T = 273 \text{ K}$. Changes in the critical breakdown distance reflect the considerable influence of both boundary surface conditions and gaseous impurities. However, the spatial investigations by themselves do not permit an unambiguous assessment of the relative importance of the surface and volume processes. For this purpose the spatial studies must be complemented by temporal investigations of the ionisation growth, which are capable of separating the fast and slow ionisation processes. The dominant slow processes are found to be associated with metastable particles which have insufficient energy to ionise gaseous impurities by the Penning process but which diffuse to the electrodes and release secondary electrons. A typical variation of the ionisation current with

time for such a case is shown in Fig. 1 *b*. On a semi-log plot (see Fig. 2 *a*) it can be seen that the ionisation current varies exponentially with a decay constant $1/T$. Using the Molnar (1951 *a*) analysis this can be related to the fundamental time constant $1/\tau$ of the metastable species through the relation

$$\frac{1}{\tau} = \frac{\pi^2 D_m p}{pd^2} + G = \frac{1}{T} \frac{I_T}{I_F} \quad (1)$$

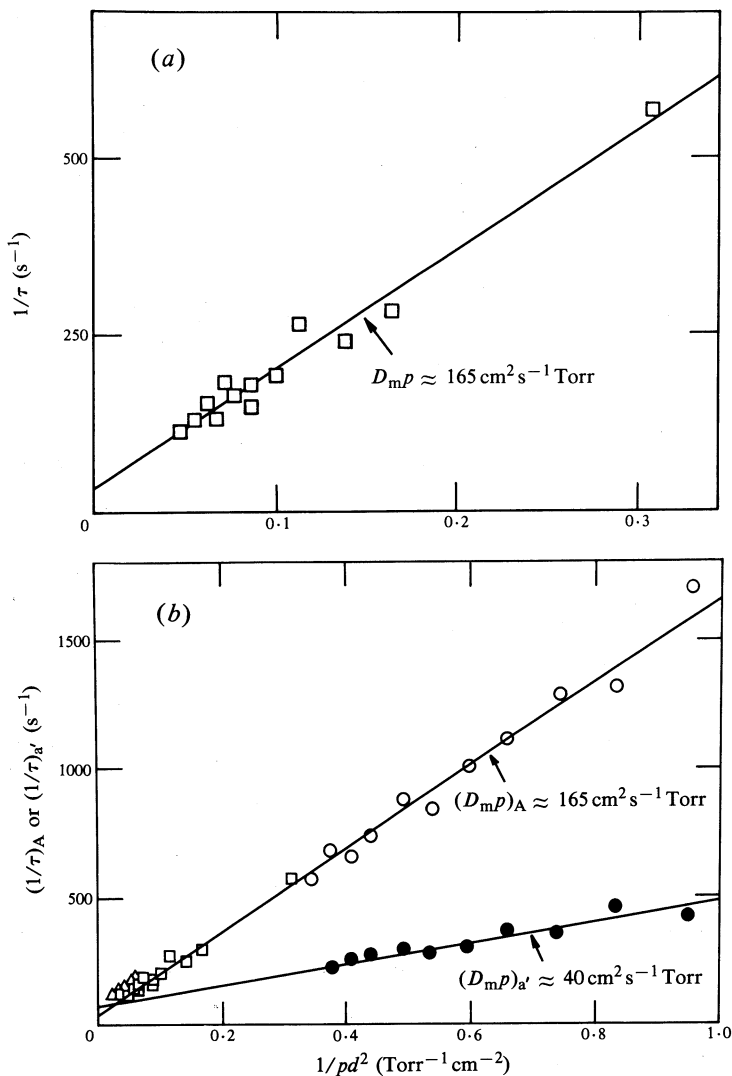


Fig. 3. (a) Fundamental time constant $1/\tau$ plotted against $1/pd^2$ for an unbaked or moderately baked system yielding a $D_m p$ value for $N_2(A^3\Sigma_u^+)$ metastable particles. (b) Corresponding $1/\tau$ versus $1/pd^2$ plots for high purity gas (baked UHV system) for A (open circles) and A' (solid circles) of Fig. 2 *b*. The square and triangle values were obtained from decay curves showing a single exponential time dependence and lower purity gas (unbaked system).

where G is the volume quenching parameter. In this way a possibility exists for identifying the particles responsible for the $I-t$ characteristic provided independent values of the derived diffusion coefficient D_m are available. Fig. 3*a* shows a summary of many experiments yielding values of $1/\tau$ versus $1/pd^2$ in unbaked or moderately baked systems from which a value for $D_m p = 165 \text{ cm}^2 \text{ s}^{-1} \text{ Torr}$ has been derived. This value was obtained using the approximate relation (1). When higher order approximations in the Molnar theory are used a value of $153 \text{ cm}^2 \text{ s}^{-1} \text{ Torr}$ is obtained. Such a value is consistent with the $\text{N}_2(\text{A } ^3\Sigma_u^+)$ metastable particle being the predominant contributor to the ionisation current. The radiative lifetime ($\sim 0.5 \text{ s}$) of this metastable particle is also consistent with the time scale of these observations.

Improved gas purity (curves II in Fig. 1*a*) leads to the results shown in Fig. 2*b*. The curvature in the semi-log plot is due to the sum of the two exponential components shown as A and a' respectively. Analysis of curve A yields a value for $D_m p$ of $165 \text{ cm}^2 \text{ s}^{-1} \text{ Torr}$ and thus confirms this contribution as being that from the $\text{N}_2(\text{A } ^3\Sigma_u^+)$ state. The value of $D_m p$ derived from curve a' is $40 \text{ cm}^2 \text{ s}^{-1} \text{ Torr}$ (see Fig. 3*b*).

Unfortunately, the absence of corresponding measurements of the diffusion coefficient D_m for excited states of N_2 other than the A state precludes the possibility of an identification of the second particle by its diffusion coefficient. Furthermore, no extensive theoretical investigations of the diffusion of excited states of N_2 molecules through the parent gas have yet been made. Consequently, it is not possible to assess the nature of the intermolecular potentials that would be required for such a particle to yield a diffusion coefficient of $\sim 40 \text{ cm}^2 \text{ s}^{-1} \text{ Torr}$. Nevertheless, of those particles that could possibly be responsible for our observations, the $\text{N}_2(\text{a}' ^1\Sigma_u^-)$ particle is one that needs to be considered seriously. Preliminary considerations left doubts that the known direct electron impact excitation cross section for this state was sufficiently large for the necessary population to be established. However, the recognition (McFarlane 1965, 1966) that the $\text{N}_2(\text{a}' ^1\Sigma_u^-)$ state could also be populated via cascade processes from the vibrational levels of the $\text{N}_2(\text{a } ^1\pi_g)$ to the $v = 0, 1, 2$ levels of the a' state looked more promising. Furthermore, the time scale ($\sim 1 \mu\text{s}$) for the population of these a' vibrational levels to build up in this way (Freund 1972) and the lifetimes of these lower vibrational levels of the a' state ($\sim 0.7 \text{ s}$) are consistent with the properties required of the unidentified particle in the ionisation growth experiments.

This possibility of two-particle contributions to the ionisation growth raises the question of the relative importance of surface ionisation processes and of gas quenching mechanisms. This matter could clearly not be resolved until some procedures were established that yielded stable, reproducible electrode surfaces. These are outlined in the next section and the specific influence of trace impurities of H_2 and CO on the gas volume processes are described in Section 4.

3. Outgassing and Surface Discharge Procedures

In order to establish the procedures necessary to achieve reproducible surfaces a detailed investigation was made of the dependence of the ionisation current I on the voltage V applied across the two fixed copper electrodes at constant pressure p in the simple apparatus of Fig. 4. In such experiments the value of E/p increases progressively as V is increased.

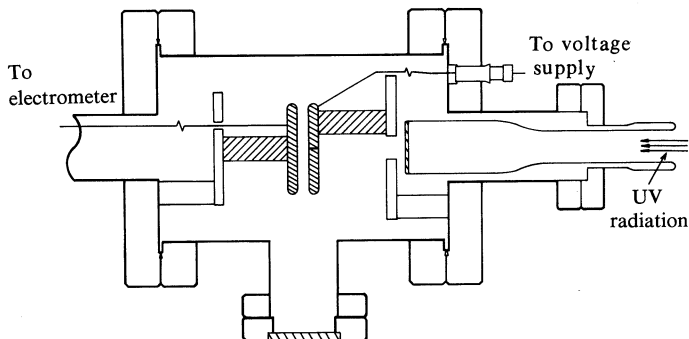


Fig. 4. Schematic diagram of the ionisation chamber used for investigations of trace impurity effects.

The conditions found to have a significant influence on the $I-V$ characteristics were:

- (i) whether or not the electrode components were vapour degreased before assembly;
- (ii) the extent of vacuum degassing at elevated temperatures;
- (iii) the extent of glow discharge treatment of the boundary surfaces in samples of pure hydrogen gas;
- (iv) the level of contamination of the samples of the original research grade nitrogen gas admitted to the ionisation chamber;
- (v) the length of time the electrode boundary surfaces were exposed to the UV radiation generated by an external mercury vapour lamp to provide the necessary initial current I_0 .

Fig. 5a summarises the results of a particular series of experiments. It was first demonstrated that, by prolonged outgassing of the apparatus and using a low current ($\sim 10 \mu\text{A}$) hydrogen glow discharge to 'clean' the copper electrode, it was possible to reduce the breakdown voltage V_s to a value as low as 250 V at a pressure of 4 Torr. The ionisation chamber was then isolated from the UHV system and the ionisation current monitored (point A to H) over some 450 h at $V = 240.2 \text{ V}$ corresponding to $E/p = 100 \text{ V cm}^{-1} \text{ Torr}^{-1}$ (see Fig. 5b). A portion of the $I-V$ curve taken at this stage is labelled 1 in Fig. 5a, the value of V_s having increased by some 10 V over this period. Subsequently, some time-lag measurements involving milliampere discharges through the gas led to curve 2, and after prolonged time-lag observations over a further period of 7 days to curve 3. The system was then re-attached to the UHV system and the gas filling line filled to a pressure of 4 Torr of pure N_2 before sharing volumes with the ionisation chamber; this led to curve 4. At this stage the whole system was pumped out and a fresh, pure sample of N_2 admitted to the ionisation chamber to yield curve 5. Finally, the glow discharge treatment in H_2 was carried out followed by re-pumping and admittance of a further fresh, pure sample of N_2 to a pressure of 4 Torr to give curve 6. In this way the gas and surface conditions appropriate to the low value of V_s of 250 V were retrieved.

Further investigations showed that provided the gas contamination was kept to a sufficiently low level, consistent and reproducible values of the breakdown voltage were observed. Any change in the value of V_s with time could be identified with

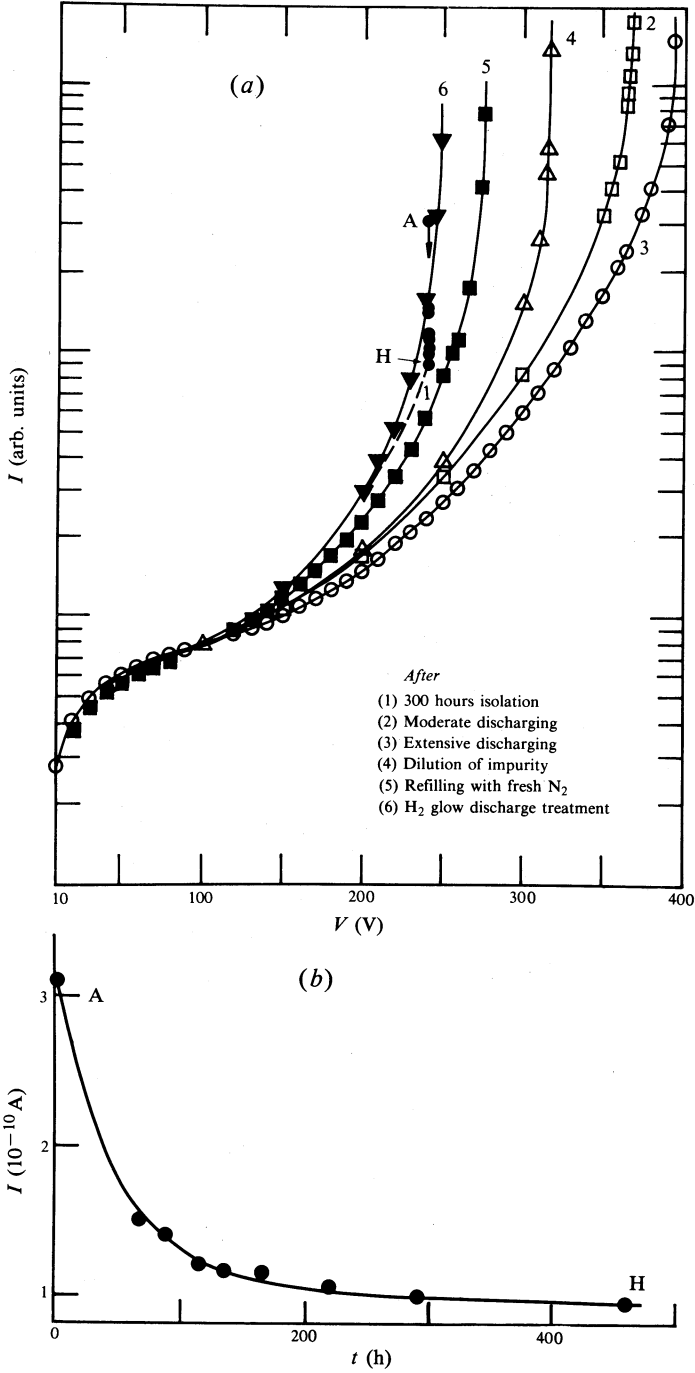


Fig. 5. (a) Curves of I versus V showing the effect of six discharge and other treatments on the threshold breakdown voltage for $p = 4$ Torr and $d = 0.6$ cm. (b) Variation of the ionisation current with time after admission of N_2 in the sealed-off ionisation chamber.

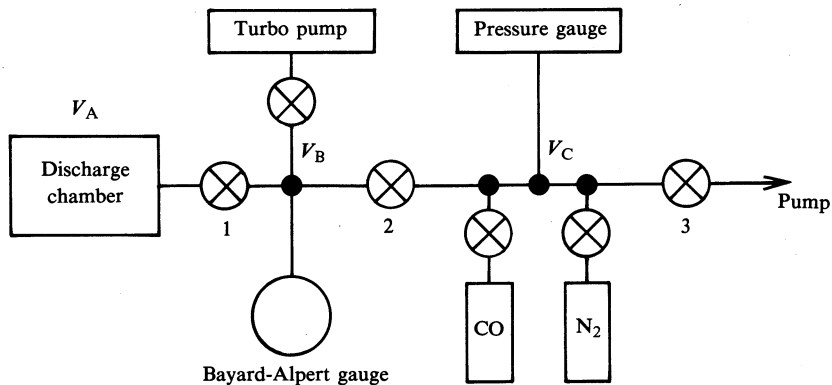


Fig. 6. Schematic diagram of the UHV system used for investigations of trace impurity effects.

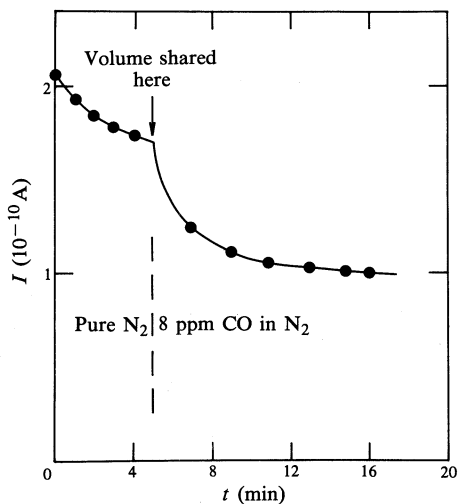


Fig. 7. Variation of current with time showing the consequences of sharing a contaminated sample of N₂ with a pure sample.

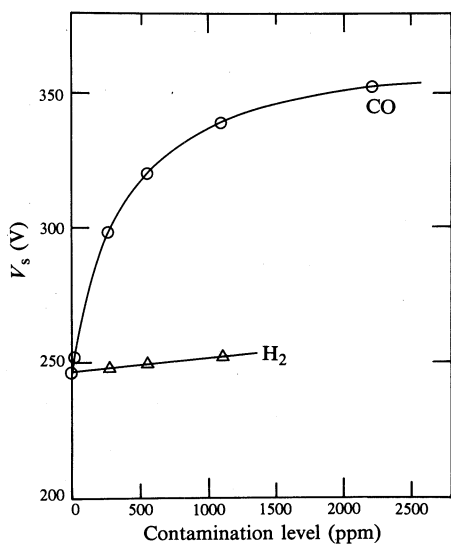


Fig. 8. Variation of V_s , obtained from a plot of V versus I , with concentrations of trace impurities of both CO and H₂ in the N₂ sample ($p = 4.0$ Torr).

changes in the gas contamination and not to an irreversible change in the electrode surfaces. Indeed, over a period of 5 days, changes in V_s as small as 2.6 V could be attributed to changes in the gas contamination only, the original V_s value being retrieved by admitting fresh, uncontaminated gas.

The influence of UV irradiation was established in the course of monitoring changes in $I-V$ characteristics over long periods of time as gas contamination levels gradually built up in the sealed-off ionisation chamber. Small changes in the breakdown voltage depended on whether the electrode surfaces were irradiated continuously or only for the period required to record the $I-V$ data. Experience has now shown that, depending on the history of the preparation of the ionisation chamber for pure gas studies, rapid changes can occur in the value of V_s when the quartz window is continuously UV irradiated. As will become clear in Section 4, the cause is believed to be associated with desorption of CO. Since there is considerable evidence that CO is not adsorbed on clean copper surfaces (Tracy 1972; Watanabe and Wissman 1984) at room temperature the source of the desorbed CO is most probably the quartz window and the stainless steel of the manifold (Vig 1985).

4. Effects of Trace Impurities of CO and H₂

Having established reproducible surface conditions, and consequently stable values of ionisation current and breakdown voltage, it was possible to examine quantitatively the influence of ppm levels of trace impurities on the measured values of these quantities. For this purpose the UHV system shown schematically in Fig. 6 was used. The doping of the N₂ samples was carried out by a volume sharing technique. By using particular volume combinations and the measurement of initial and final pressures it was established that $V_B/V_C = 1.226$ and $V_B/V_A = 0.5386$; thus, $V_B = 1.226 V_C$ and $V_A = 2.277 V_C$.

For the doping tests the whole system was pumped to a base pressure of 1.8×10^{-8} mbar, and pure N₂ admitted to a pressure of 4 Torr. Volume V_A was isolated and the volumes V_B and V_C pumped out to 5.3×10^{-5} mbar before admitting a quantity of pure CO to volumes $V_B + V_C$ and pumping the gas out to a pressure of 8×10^{-5} mbar as measured on the ionisation gauge. Adding pure N₂ to a pressure of 4 Torr resulted in a sample doped with ~ 15 ppm of CO.

The doping test consisted of monitoring the ionisation current in the volume V_A to ensure a stable reading at $V = 240.2$ V ($\sim E/p = 100$ V cm⁻¹ Torr⁻¹) before opening valve 1 and noting the changes in the current I as the doped gas diffused into the pure sample (Fig. 7). When equilibrium was established the level of dopant was ~ 8 ppm. The corresponding $I-V$ curve was then measured and V_s determined. The procedure was repeated for dopant levels up to ~ 2200 ppm, the variation of V_s with dopant level being shown in Fig. 8. Subsequently, similar tests were carried out for H₂ as the impurity in pure N₂. The dramatic differences in the quenching influence of CO compared with H₂ are clearly seen in these experiments and the series of $I-V$ curves obtained for CO (Fig. 9) shows that a change in V_s of 106 V can be attributed to the quenching action of CO on excited states of N₂. The corresponding changes due to similar levels of H₂ contamination amounted to only ~ 5 V. The effects were shown to be reversible by diluting the contaminated gas with pure N₂ by volume sharing, thus confirming that these particular changes in ionisation current were associated with gas volume processes and not with surface phenomena.

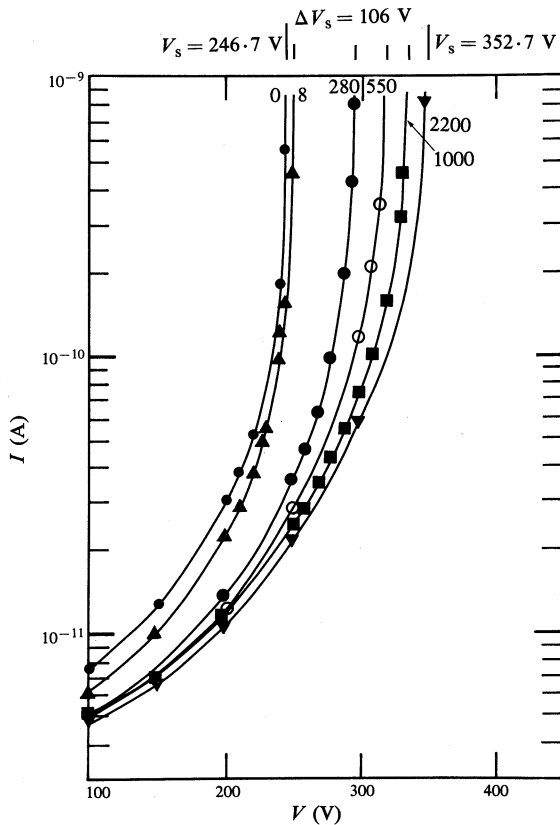


Fig. 9. Curves of I versus V for CO doping tests (in ppm) in pure N_2 .

5. Spatial Ionisation Growth at Constant Electrode Separation or Gas Pressure

I versus p Studies

Fig. 10 shows the variation of ionisation current I with gas pressure p observed in the ionisation chamber of Fig. 4, for a constant value of $E/p = 100 \text{ V cm}^{-1} \text{ Torr}^{-1}$ ($E/N = 282.2 \text{ Td}$). For simplicity the plane-parallel gap was set at a separation of 0.6 cm and external UV irradiation was admitted onto the cathode surface via a single 0.5 mm diameter circular hole in the anode. The circles represent ionisation currents measured before any outgassing of the UHV system, whilst the triangles are those observed after the system was outgassed. The critical breakdown voltages for these two sets of observations were ~ 960 and $\sim 480 \text{ V}$ respectively. These are very much the same as those observed for the same E/p in the corresponding $I-d$ results shown in Fig. 1a for both copper and Au-film surfaces in a stainless-steel UHV system. Consequently, we expect to be able to account for the measurements made before outgassing (i.e. the circles in Fig. 10) in terms of a single-particle $N_2(A^3\Sigma_u^+)$ mechanism.

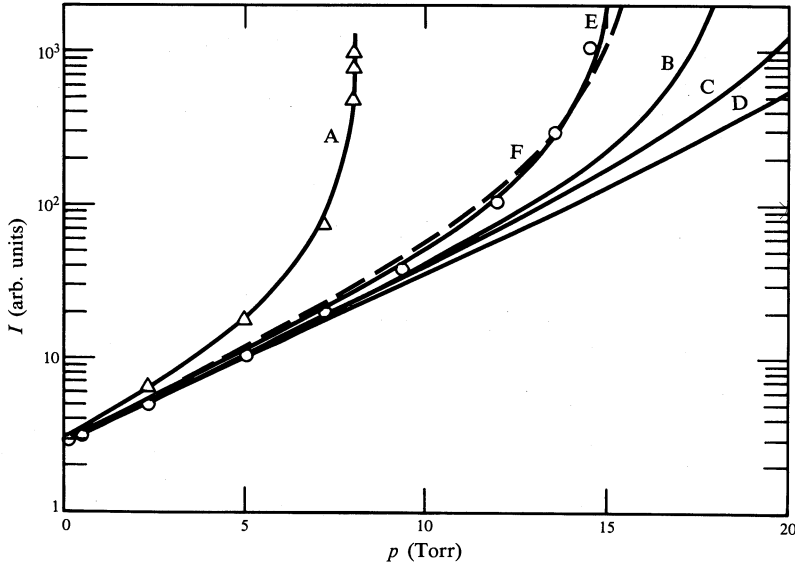


Fig. 10. Comparison of computed ionisation current versus gas pressure with corresponding experimental measurements. *Experimental:* $E/p_{273} = 100 \text{ V cm}^{-1} \text{ Torr}^{-1}$; circles, before the UHV system was outgassed; triangles, after the system was outgassed. *Computed:* (A) High purity gas; $\mu/\alpha = 0.05$; based on a one- or two-particle mechanism (see Table 1). (B) High purity gas; $\mu/\alpha = 0.05$, $A(^3\Sigma_u^+)$ only present; $\alpha_m \eta_m/p = 1.87 \times 10^{-2} \text{ cm}^{-1} \text{ Torr}^{-1}$. (C) Low purity gas; $\mu/\alpha = 0.6$, $A(^3\Sigma_u^+)$ only present; $\alpha_m \eta_m/p = 1.87 \times 10^{-2} \text{ cm}^{-1} \text{ Torr}^{-1}$. (D) Low purity gas; $\mu/\alpha = 0.6$, $A(^3\Sigma_u^+)$ only present; $\alpha_m \eta_m/p = 2.43 \times 10^{-3} \text{ cm}^{-1} \text{ Torr}^{-1}$. (E) High purity gas; $\mu/\alpha = 0.05$, $A(^3\Sigma_u^+)$ only present; $\alpha_m \eta_m/p = 0.040 \text{ cm}^{-1} \text{ Torr}^{-1}$. (F) Low purity gas; $\mu/\alpha = 0.6$, $A(^3\Sigma_u^+)$ only present; $\alpha_m \eta_m/p = 0.065 \text{ cm}^{-1} \text{ Torr}^{-1}$.

Such calculations require information about the parameters α/p , $\omega_{\text{ph}} + \omega_+$ and f_{mk} , as well as $\alpha_m \eta_m/p$ and μ/α , all of which have been defined and considered elsewhere (Haydon and Williams 1973*a*, 1973*b*, 1973*c*). Since the *gas purity* conditions before outgassing were believed to be similar to those that existed in the earlier measurements by Haydon and Williams (1976), we have assumed in the first instance the values of the parameters appropriate to those experiments. These have been taken from their Table 1 and yield curve C. It should be noted that the values given in our Table 1 were appropriate to a Au-film cathode. As pointed out above the differences between the Au-film and copper surfaces were observed to be much smaller in the stainless-steel UHV systems and on this basis a value of $\alpha_m \eta_m/p = 1.87 \times 10^{-2} \text{ cm}^{-1} \text{ Torr}^{-1}$ for the copper surface is not likely to be significantly in error. Nevertheless, on the basis that the value of η_m for copper may have been a factor 7.7 times smaller than for the Au-film (see Haydon and Williams 1973*c*), the calculations have been repeated for $\alpha_m \eta_m/p = 2.43 \times 10^{-3} \text{ cm}^{-1} \text{ Torr}^{-1}$ (see curve D).

In each case the predicted values of current are too small. If, because of the use of a stainless-steel system, the level of impurity was much reduced and the value of μ/α was much smaller than 0.6, then the ionisation currents should be larger. Consequently we have also computed the I versus p curve on the assumption that $\mu/\alpha = 0.05$ (see curve B). There is still a large discrepancy with the observed values

Table 1. Values of parameters used in various tests of agreement between computed and observed ionisation currents

The η_m values shown are those based on the assumption that the values of $(\alpha_m/p)_A$ and $(\alpha_m/p)_{a'}$ are 5.24 and $0.587 \text{ cm}^{-1} \text{ Torr}^{-1}$ respectively (H. Tagashira and Y. Ohmori, personal communication 1985)

V_s (V)	Type of experiment ^A	Gas purity	μ/α	Cathode surface	Pressure (Torr)	Electrode separation (cm)	One particle		$\alpha_m \eta_m / p$ ($\text{cm}^{-1} \text{ Torr}^{-1}$)	Two particle		$(\eta_m)_{a'}$
							$(\alpha_m \eta_m / p)_A$ ($\text{cm}^{-1} \text{ Torr}^{-1}$)	$(\eta_m)_A$		$(\eta_m)_A$	$(\alpha_m \eta_m / p)_{a'}$ ($\text{cm}^{-1} \text{ Torr}^{-1}$)	
~480	<i>I vs p</i> (10A)	High	0.05	Cu		0.6	0.187	3.6×10^{-2}	0.104	2×10^{-2}	0.083	0.14
	<i>I vs p</i> (10B)	High	0.05	Cu		0.6	0.0187	3.6×10^{-3}				
~950	<i>I vs p</i> (10E)	High	0.05	Cu		0.6	0.040	7.6×10^{-3}				
~425	<i>I vs d</i> (11D)	High	0.05	Au	5		0.213	4.1×10^{-2}	0.104	2×10^{-2}	0.109	0.19
	<i>I vs p</i> (10C)	Low	0.6	Cu		0.6	0.0187	3.6×10^{-3}				
	<i>I vs p</i> (10D)	Low	0.6	Cu		0.6	0.00243	4.8×10^{-4}				
	<i>I vs p</i> (10F)	Low	0.6	Cu		0.6	0.065	1.2×10^{-2}				
~1050	<i>I vs d</i> (11A)	Low	0.6	Au	5		0.0187	3.6×10^{-3}				

^A See e.g. Fig. 10, curve A.

and it is necessary to increase $(\eta_m)_A$ to a value of 7.6×10^{-3} to yield good agreement (see curve E). By contrast it is not possible, with a value $\mu/\alpha = 0.6$, to match the *shape* of the I versus p curve simply by increasing $(\eta_m)_A$ to a sufficiently large value. Curve F shows the results for a value $(\eta_m)_A = 1.2 \times 10^{-2}$.

Turning to the measurements (triangles in Fig. 10) made after the UHV system was outgassed, it is clear that the value of $(\eta_m)_A$ for the copper surface must increase substantially if this single-particle mechanism is entirely responsible for the ionisation growth. Further calculations (see curve A and Table 1) show that an order of magnitude increase in η_m is required.

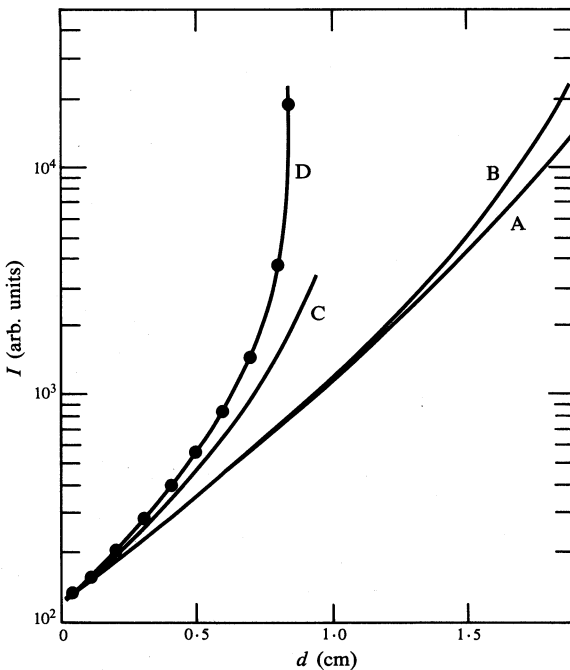


Fig. 11. Experimental and computed values of I versus d for $E/p = 100 \text{ V cm}^{-1} \text{ Torr}^{-1}$ ($E/N = 282.8 \text{ Td}$), $p = 5 \text{ Torr}$ and Au-film cathodes. The experimental values (circles) are for $\mu/\alpha \rightarrow 0$, while the computed curves are for: (A) $\alpha_m \eta_m = 0.094 \text{ cm}^{-1}$ and $\mu/\alpha = 0.6$; (B) $\alpha_m \eta_m = 0.094 \text{ cm}^{-1}$ and $\mu/\alpha = 0.05$; (C) $\alpha_m \eta_m = 0.66 \text{ cm}^{-1}$ and $\mu/\alpha \rightarrow 0$; (D) $\alpha_m \eta_m = 1.07 \text{ cm}^{-1}$ and $\mu/\alpha \rightarrow 0$.

I versus d Studies

The extreme sensitivity of the quantity η_m to the state of the electrode surface clearly poses some difficulties when attempting to extend the kind of predictions summarised so far in Fig. 10. The problem becomes even more severe when it is anticipated that the ionisation behaviour may be determined by the combined action of two metastable particles at the boundary surfaces. In view of this and with

the knowledge gained from the results of Sections 3 and 4, some further extensive investigations of both the spatial (I versus d) and temporal (I versus t) growth of ionisation have been undertaken and will be reported in a further paper. For the purposes of the present discussion we report (circles in Fig. 11) one recent set of such I versus d observations made at $E/p = 100 \text{ V cm}^{-1} \text{ Torr}^{-1}$. The freshly prepared surfaces in this experiment did not reveal the very large differences between the Au and Cu surfaces observed in the earlier experiments of Haydon and Williams (1973c). For comparison with these recent observations we include curve A of I versus d with the Au-film cathode that yielded the $\bar{\omega}(d)$ versus αd information of Fig. 3 in Haydon and Williams (1976). In those experiments, $\bar{\omega}(d)$ values were $\lesssim 0.04 \text{ cm}^{-1}$ and $\mu/\alpha = 0.6$, and only the $\text{N}_2(\text{A}^3\Sigma_u^+)$ particle was considered to contribute to the ionisation growth, since no evidence in the corresponding temporal data suggested otherwise. The value of $\alpha_m \eta_m/p$ appropriate to those particular measurements was $1.87 \times 10^{-2} \text{ cm}^{-1} \text{ Torr}^{-1}$ giving for $p = 5 \text{ Torr}$ the value $\alpha_m \eta_m = 0.094 \text{ cm}^{-1}$. Again, we can compute values to be expected if the gas purity is improved so that $\mu/\alpha = 0.05$, the surface ionisation efficiency η_m remains unaltered and $\alpha_m \eta_m$ remains at the value 0.094 cm^{-1} (see curve B in Fig. 11). The relatively small change in I versus d values this causes is consistent with the relative magnitudes of the volume and surface effects observed in Section 4 and leads to the conclusion that a very large change in η_m must accompany the improved gas purity if the single-particle mechanism is to account for the experimental results shown by the circles in Fig. 11. In proceeding further with our attempts to establish the mechanisms responsible for these dramatic changes, we should take note of the demonstrated sensitivity of the ionisation behaviour of N_2 to trace impurities of CO (see Section 4). We are then immediately faced with a dilemma which can be simply stated:

(i) Not only is the $\text{N}_2(\text{A}^3\Sigma_u^+)$ metastable particle quenched by CO (Young *et al.* 1969), but so also are the $\text{N}_2(\text{a}^1\pi_g)$ and the $\text{N}_2(\text{a}'^1\Sigma_u^-)$ particles (Golde and Thrush 1972; Golde 1975). Consequently, we cannot on these grounds alone immediately reject either the single- or the two-particle explanation.

(ii) On the other hand, whilst the spatial characteristics of the ionisation growth could be accounted for if the single-particle surface ionisation efficiency $(\eta_m)_A$ increased dramatically with improved purity, we have no plausible explanation at this stage that would account for the temporal characteristics of Fig. 2b.

(iii) By contrast, a two-particle mechanism is capable, in principle, of accounting for the temporal observations, but we have yet to show that it is capable of providing a plausible explanation for the spatial observations reported in this paper. We examine this in the next section.

6. Interpretation of I versus d and I versus p Data Using Two Metastable Particles

The absence of reliable information about the values of either the excitation coefficients for metastable particles α_m/p , or of the surface ionisation efficiency η_m , has inhibited assessments of the plausibility of both the single- and two-particle mechanisms. No measurements are available for values of $(\eta_m)_A$ and $(\eta_m)_{a'}$ for the $\text{N}_2(\text{A}^3\Sigma_u^+)$ and $\text{N}_2(\text{a}'^1\Sigma_u^-)$ states on Au-film and Cu surfaces as used in these experiments. However, Borst (1972) has given values for secondary electron yields as a function of metastable excitation energy for Auger ejection of electrons from Cu-Be-O surfaces and these lie on a smooth curve. For the $\text{A}^3\Sigma_u^+$ and $\text{a}^1\pi_g$

states the η_m values are $\sim 10^{-3}$ and $\sim 10^{-2}$ respectively. From this information we might anticipate the ratio of $(\eta_m)_a/(\eta_m)_A$ to be ~ 10 , although the absolute values for our particular surfaces remain unknown in the absence of reliable information about the excitation coefficients. Fortunately, several investigations to determine the values of excitation rates (α_{ex}/p) in N_2 have been made recently. Z. Petrović (personal communication 1983) provided some preliminary data for values of α_m/N for production of $N_2(A^3\Sigma_u^+)$ particles based on direct electron impact excitation and cascade processes from the upper B, C and W states of N_2 yielding a value of $1.71 \times 10^{-16} \text{ cm}^2$ at $E/p = 100 \text{ V cm}^{-1} \text{ Torr}^{-1}$. The corresponding value for α_m/N for the $N_2(a^1\Sigma_u^-)$ state, by both direct electron impact excitation (Ajello 1970; Borst 1972), together with a further 20% contribution from the $N_2(a^1\pi_g)$ state (see Section 2 and also Freund 1972) gave $0.174 \times 10^{-16} \text{ cm}^2$. More recent calculations (H. Tagashira and Y. Ohmori, personal communication 1985) yielded values of 1.48×10^{-16} and $0.166 \times 10^{-16} \text{ cm}^2$ respectively.

In the following discussion we assume the values provided by Tagashira and Ohmori. In this way it is possible, having established the values of $\bar{\omega}(d)$ appropriate to the observations of I versus p or of I versus d to deduce values for the surface efficiencies $(\eta_m)_A$ and $(\eta_m)_a$. These can then be examined in the light of the Borst data to assess the plausibility of an explanation of the spatial ionisation data in terms of two such metastable particles.

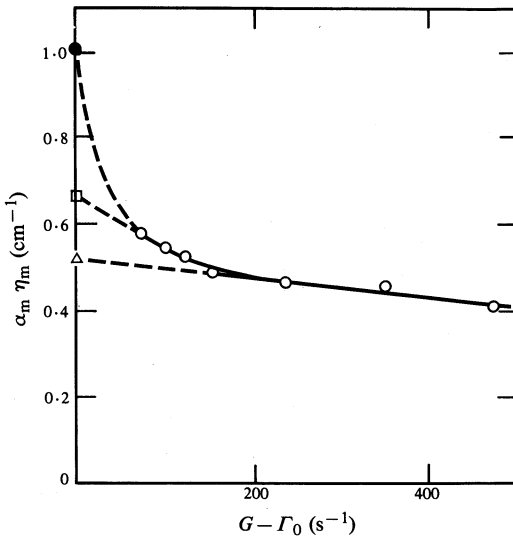


Fig. 12. Experimental values (open circles) of $\alpha_m \eta_m$ versus $G - \Gamma_0$ (from Haydon and Williams 1973c) showing the basis of extrapolated values used to compute the I versus d values in Fig. 11, for $E/p = 100 \text{ V cm}^{-1} \text{ Torr}^{-1}$, $p = 5.02 \text{ Torr}$, and Au-film cathodes. The $\alpha_m \eta_m$ values corresponding to $G - \Gamma_0 = 0$ were 0.52 (triangle), 0.66 (square) and 1.07 (solid circle).

The two sets of data appropriate to such analysis are the I versus p and I versus d data corresponding to high purity conditions for which $\mu/\alpha = 0.05$. As a starting point we take the experimental data from Fig. 6 of Haydon and Williams (1973c) which shows $\alpha_m \eta_m$ versus $G - \Gamma_0$ (see our Fig. 12). Those experiments were undertaken with a freshly prepared Au-film cathode surface and yielded $\bar{\omega}(d)$ values at $E/p = 100 \text{ V cm}^{-1} \text{ Torr}^{-1}$ of $\sim 0.2 \text{ cm}^{-1}$, indicating that the surface conditions were much closer to those existing when the I versus p and I versus d measurements of Figs 10 and 11 were made at high purity, for which the $\bar{\omega}(d)$ values were $\sim 0.4 \text{ cm}^{-1}$. By contrast the values of $\bar{\omega}(d)$ in the experiments reported by

Haydon and Williams (1976), and which led to Table 1 here, were $\sim 0.04 \text{ cm}^{-1}$, i.e. some five to six times smaller than in the 1973 experiments, due, we believe, to surface contamination and reduced η_m values following prolonged experiments with an aged gold film.

We now extrapolate the data of Fig. 12 to low values of G , corresponding to very pure gas conditions as $\mu/\alpha \rightarrow 0$. The linear extrapolation of the 'impure' values of $\alpha_m \eta_m$ for the $\text{N}_2(\text{A}^3\Sigma_u^+)$ particle (i.e. $G \geq 150 \text{ s}^{-1}$) gave $\alpha_m \eta_m \sim 0.52 \text{ cm}^{-1}$ (triangle). A corresponding linear extrapolation of the 'pure' values (i.e. $G \leq 150 \text{ s}^{-1}$) gave $\alpha_m \eta_m \sim 0.66 \text{ cm}^{-1}$ (square), it now being assumed that the increase (0.14 cm^{-1}) is to be attributed to the $\text{N}_2(\text{a}'^1\Sigma_u^-)$ particle. The computed I versus d values using $\alpha_m \eta_m = 0.66 \text{ cm}^{-1}$ (curve c in Fig. 11) fell short of the observations. In order to yield the observed ionisation currents (curve D and circles), the contribution from the second $\text{N}_2(\text{a}'^1\Sigma_u^-)$ particle had to be increased from $\alpha_m \eta_m = 0.14$ to 0.55 cm^{-1} , corresponding to the curved extrapolation in Fig. 12 (solid circle) rather than the assumed linear form. Recognising that these assumptions are made simply to establish the plausibility of a two-particle explanation we can proceed to assess this by examining the consequences of these assumptions for the values of the surface efficiencies $(\eta_m)_A$ and $(\eta_m)_{a'}$. This we can do on the basis of the values for $(\alpha_m/N)_A$ and $(\alpha_m/N)_{a'}$ provided by Tagashira and Ohmori. This same value for $(\alpha_m/N)_A$ can also be used to establish the value of $(\eta_m)_A$ that would be required on the basis of a single-particle [i.e. $\text{N}_2(\text{A}^3\Sigma_u^+)$] mechanism. The results of these analyses are summarised in Table 1.

It can be seen that for our low purity conditions and a single A-particle mechanism, the surface ionisation efficiency $(\eta_m)_A$ is $\sim (3-8) \times 10^{-3}$ compared with Borst's value of $\sim 8 \times 10^{-4}$ to 3×10^{-3} . For high purity conditions this value would have to increase by a factor of ~ 5 for the I versus p data and an order of magnitude for the I versus d data. If two particles are assumed the $(\eta_m)_A$ value still needs to be an order of magnitude more than the Borst value and $(\eta_m)_{a'} \approx 10 \times (\eta_m)_A$. The ratio $(\eta_m)_{a'}/(\eta_m)_A$ is then consistent with the Borst secondary electron yield curve, although the absolute values are both an order of magnitude larger than those quoted by Borst.

In the absence of direct measurements of η_m appropriate to our particular surfaces, it is not fruitful to pursue the analysis of the present spatial information any further. It does appear, however, that the action of the two metastable particles $\text{N}_2(\text{A}^3\Sigma_u^+)$ and $\text{N}_2(\text{a}'^1\Sigma_u^-)$ may provide a plausible explanation of the observations so far. The problem of accounting for the low apparent value of the diffusion coefficient $D_m p \sim 40 \text{ cm}^2 \text{ s}^{-1} \text{ Torr}$ has still to be addressed. Further temporal ionisation data, obtained using surfaces prepared by the procedures described in Sections 3 and 4, have now been obtained and are being critically analysed. A further paper reporting the results of these and related investigations will be submitted for publication in due course.

7. Conclusions

The present investigation has shown that a two-particle mechanism based on contributions from $\text{N}_2(\text{A}^3\Sigma_u^+)$ and $\text{N}_2(\text{a}'^1\Sigma_u^-)$ metastable states is a plausible explanation of the observed spatial characteristics of ionisation growth in highly pure N_2 samples. Whilst it has been confirmed that the spatial behaviour is highly sensitive

to the presence of ppm levels of CO, this does not itself resolve the relative magnitudes of the contributions from these two particles because information about the change of surface ionisation efficiencies with prolonged outgassing procedures is not available.

If the two-particle mechanism considered here represents a plausible explanation of the observations, then further investigations of the temporal growth are desirable to resolve the underlying explanation for the unusually low value of the diffusion coefficient $(D_m p)_{a'} \sim 40 \text{ cm}^2 \text{ s}^{-1} \text{ Torr}$. Coupled with such measurements, it could be desirable to monitor the corresponding changes in surface composition and surface ionisation efficiencies. Further work is continuing to obtain more direct evidence for the existence of the a' metastable particle. Independent theoretical confirmation of our apparent measured value of the diffusion coefficient, based on appropriate information about the intermolecular forces controlling the diffusion of the a' particle through its parent gas, would be helpful.

Acknowledgments

This work has been supported mainly by the Australian Research Grants Committee. The authors wish to acknowledge further support received from both the Australian Institute for Nuclear Science and Engineering and the Electrical Research Board of Australia. One of us (S.C.H.) wishes to acknowledge the support of the AMP Laboratories at the Research School of Physical Sciences in making its facilities available for the investigation during the tenure of a Visiting Fellowship at the Australian National University. The helpful comments by Drs S. J. Buckman and B. Lohmann on this paper are also acknowledged.

References

- Ajello, J. M. (1970). *J. Chem. Phys.* **53**, 1156–65.
Borst, W. L. (1972). *Phys. Rev. A* **5**, 648–56.
Ernest, A., and Haydon, S. C. (1983). Proc. XVIth Int. Conf. on Phenomena in Ionized Gases, Dusseldorf, Aug. 1983 (Eds W. Botticher *et al.*), pp. 132–3 (Henkel: Dusseldorf).
Folkard, M. A., and Haydon, S. C. (1973). *J. Phys. B* **6**, 214–26.
Freund, R. S. (1972). *J. Chem. Phys.* **56**, 4344–51.
Golde, M. F. (1975). *Chem. Phys. Lett.* **31**, 348–50.
Golde, M. F., and Thrush, B. A. (1972). *Proc. R. Soc. London A* **330**, 97–108.
Haydon, S. C., and Williams, O. M. (1972). *J. Phys. D* **5**, L79–81.
Haydon, S. C., and Williams, O. M. (1973*a*). *J. Phys. B* **6**, 227–31.
Haydon, S. C., and Williams, O. M. (1973*b*). *J. Phys. B* **6**, 1856–65.
Haydon, S. C., and Williams, O. M. (1973*c*). *J. Phys. B* **6**, 1866–80.
Haydon, S. C., and Williams, O. M. (1976). *J. Phys. D* **9**, 523–36.
Krisch, H. (1968). *Z. Phys.* **208**, 322–37.
McFarlane, R. A. (1965). *Phys. Rev. A* **140**, 1070–1.
McFarlane, R. A. (1966). *IEEE J. Quant. Electron.* **8**, 229–32.
Molnar, J. P. (1951*a*). *Phys. Rev.* **83**, 933–40.
Molnar, J. P. (1951*b*). *Phys. Rev.* **83**, 940–52.
Tracy, J. C. (1972). *J. Chem. Phys.* **56**, 2748–54.
Vig, J. R. (1985). *J. Vac. Sci. Technol. A* **3**, 1027–34.
Watanabe, M., and Wissman, P. (1984). *Surf. Sci.* **138**, 95–112.
Young, R. A., Black, G., and Slinger, T. G. (1969). *J. Chem. Phys.* **50**, 303–11.